

High-frequency broadband matched field processing in the 8-16 kHz band

Paul Hursky
Science Applications International Corporation
10260 Campus Point Drive
San Diego, CA 92121 USA
paul.hursky@saic.com

Michael B. Porter
Science Applications International Corporation
10260 Campus Point Drive
San Diego, CA 92121 USA
michael.b.porter@saic.com

Martin Siderius
Science Applications International Corporation
10260 Campus Point Drive
San Diego, CA 92121 USA
thomas.martin.siderius@saic.com

Vincent Keyko McDonald
Space and Naval Warfare Systems Center, San Diego
53560 Hull Street
San Diego, CA 92152-5001
keyko.mcdonald@navy.mil

Abstract- We will show model-based localization results at 8-16 kHz using a single hydrophone in several shallow water environments, with successful tracking out to 3 km. It is very difficult to produce accurate replicas of the field at these high frequencies, due to sensitivity to small bathymetric features, surface motion (waves), and water column fluctuations. To reduce this sensitivity, we match the envelope of the field in the time domain, using the Bellhop ray tracing model to calculate replicas. At these high frequencies, ray tracing is a viable approach. SignalEx tests have been conducted in a variety of shallow water coastal environments to relate acoustic communications performance to oceanographic conditions. A fixed receiver and a transmitter drifting out to minimum detectable ranges were used. Waveforms to probe the channel in the 8 to 16 kHz band were transmitted at regular intervals. These signals were initially used to study the channel and subsequently to test our source localization algorithms. Working in the time domain enables the fluctuations to be directly observed as changes in the times of arrival. After aligning a sequence of probe pulses on the stabler initial arrivals, the pattern of fluctuations in the amplitudes and arrival times of the later arrivals can be observed. These fluctuations cause mismatch between the data and the replicas with which the data is being correlated, unless they are incorporated into the model of the signal. We will present measurements of the time-varying channel response and source localization results from two shallow water sites: the New England Front area, and a site off the coast of La Jolla in San Diego, California.

I. INTRODUCTION

Over the last 20 years there has been a great deal of research on using or embedding acoustic models in signal processing algorithms. An example application is for vertical or horizontal line arrays in which the spatial and temporal multipath structure is used to determine the location of a source in the ocean waveguide.

The terminology for this work is not standardized. We use the term 'model-based' processing to refer to any technique that uses a computer model of acoustic propagation in the ocean waveguide. This term encompasses 1) matched-field processing, which exploits the phase-amplitude structure of some small set of narrowband signals

(see [1], [2], and [3]), 2) back-propagation or time-reversal techniques which use a computer model to propagate the field observed on the receive array and (under certain conditions) refocus it at the source location (see [4], [5], [6], and [7]), 3) single-phone correlation processing, which exploits the temporal multipath structure (see [8], [9], [10], [11], [12], [13], and [14]). These techniques are all closely related and in some cases actually identical. However, they provide a different jumping off point and sometimes lead to different insights about how to exploit the space-time structure of the acoustic field.

Our interest here is in extending these techniques to significantly higher frequencies (previously, [15] demonstrated source localization at a mid-frequency range). Higher frequency arrays can be attractive because they can provide high spatial resolution in a small space. Alternatively, work at this band is motivated by interest in sources such as dolphins or AUVs with a signature in this band. Finally, further incentive to explore applications in this band is due to the ambient noise background being significantly lower at high frequencies than in lower bands (where the clutter is dominated by surface shipping).

The first issue that arises is that of understanding qualitatively the propagation physics in this band. Should we expect distinct echoes from the surface and bottom? Might the combined effects of surface and bottom roughness; small-scale ocean variability; source/receiver motion; and near-surface bubbles yield a diffuse smear of acoustic energy? The answers to these questions are partially contained in the literature, although most of the studies have been devoted to single boundary interactions and/or the back-scattered field. As we will show, our experiments at a variety of typical shallow water sites reveals a clear set of surface and bottom echoes rising well above the reverberant haze.



Figure 1. Telesonar testbed hardware.

The second issue is whether we can predict the field accurately enough to localize a source using the echo pattern as a fingerprint of target location. Our results demonstrate that source localization at high frequencies is possible out to ranges of several kilometers using just a single phone. However, special techniques must be applied to exploit the reliable features of the propagation.

From 1999 to the present, a series of data-collection experiments were performed at a number of shallow water coastal areas. Figure 1 shows a photograph of the Telesonar Testbed hardware developed at Spawar Systems Center for transmitting and recording acoustic waveforms in the 8-16 kHz band. Besides transmitting a variety of acoustic communications sequences during the SignalEx tests, probe pulses were transmitted on a regular basis to measure the impulse response of the ocean waveguide. Although some of the experiments used fixed-fixed configurations, we will discuss data in which the transmitter was allowed to drift from short range out to a range at which the signals were no longer detectable.

Section II will discuss the impulse response measurements. Section III will discuss how the impulse response function was modeled. Section IV will discuss how the observed impulse response was used to estimate source location.

II. IMPULSE RESPONSE MEASUREMENTS

Figure 2 shows two views of the waveform sequence during the SignalEx test off the coast of La Jolla on May 10, 2002. The upper plot in this figure, covering 25 minutes, shows different colored rectangles. The green rectangles represent identical probe sequences. The other colors represent various other test sequences, each of which is preceded by a probe sequence. The lower plot in this figure shows that a single probe sequence contains repeating probe waveforms. In the 2002 SignalEx tests to be discussed in this paper, there were 100 LFM chirps in each probes interval, each sweeping from 8 to 16 kHz, having a duration of 50 milliseconds, and repeating every 250 milliseconds (4 chirps/second, so 100 chirps emitted in 25 seconds).

Figure 3 shows 100 processed chirps (matched filter outputs), stacked one on top of each other. The rows of this image have been aligned by spacing them according to the known pulse repetition interval of 250 milliseconds, corrected for a constant Doppler. Each row of this image contains the envelope of the matched filter output, calculated using the known probe waveform as the matched filter replica. There are significant fluctuations in all arrivals. Figure 4 shows the same 100 chirps, but with each row aligned at the offset relative to the previous row where the maximum row-to-row cross-correlation occurs. In other words, we cross-correlate each pair of rows and offset the second of the pair to bring the cross-correlation peak to the zero lag. This method of aligning one matched filter output with respect to its predecessor is only one of many techniques we attempted, including peak picking – using a cross-correlation to align these waveforms turned out to be the most robust for this and other datasets. Because the cross-correlation is driven by the higher amplitude earlier arrivals, the fluctuations are all but removed from these earlier arrivals by this process. This enables the fluctuating relative times of arrival between these earlier and later arrivals to be clearly seen. The times of the later arrivals vary according to some process that is independent of the process governing the earliest arrivals.

Given the configuration with the receiver close to the bottom and the source in the water column, the 1st and 2nd arrivals are the direct and bottom-reflected paths, and the 3rd and 4th arrivals are surface interacting paths. Although the fluctuations seen in the 3rd and 4th arrivals (obviously strongly correlated), could be due to water column phenomena, they are probably due to the motion of the surface. Note that the horizontal scale is only 12 milliseconds. Additional arrivals were observed at later arrival times, with similarly variable arrival times (relative to the aligned earliest arrivals) and amplitudes, although these are not shown here.

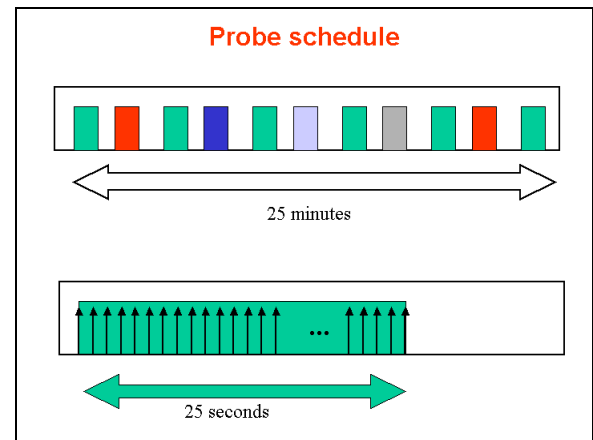


Figure 2. Diagram of overall probe schedule (upper plot) and blowup of the probes only (lower plot).

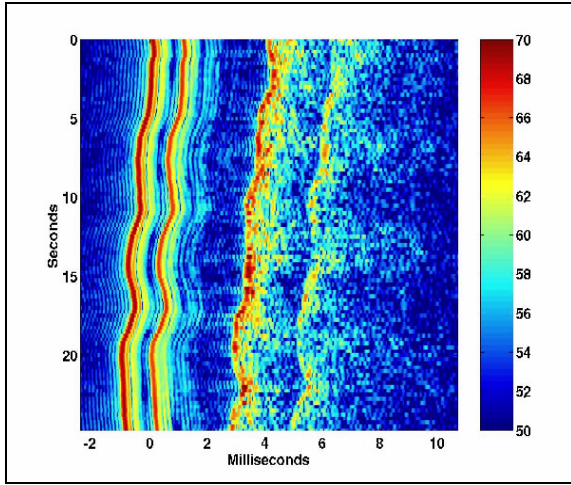


Figure 3. Stacked impulse responses, aligned according to a constant Doppler correction.

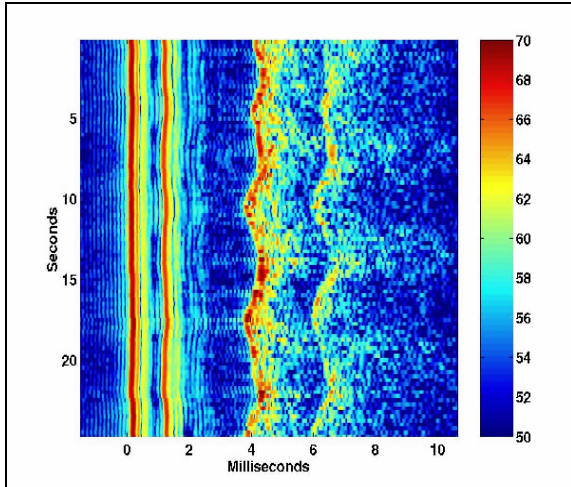


Figure 4. Stacked impulse responses, aligned by cross-correlating consecutive pairs of responses.

Figure 4 shows a single probes interval (of 25 seconds, with 100 probes, each probe an LFM chirp). Such probes intervals were repeated every two minutes for roughly six hours, while the transmitter drifted from a range of 400 to 6000 meters (as shown in Figure 6). Each of the 25-second intervals was Doppler corrected (as in Figure 3), aligned (chirp-to-chirp, as in Figure 4), and summed to form a single average impulse response function estimate. Figure 5 shows the result of stacking 90 such averages (three hours of the drift). These are the measurements that will be used to form the source location estimate.

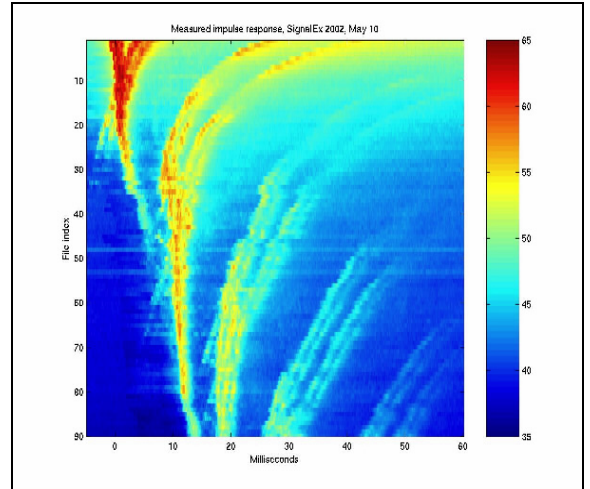


Figure 5. Measured channel impulse response as a function of range (receiver depth of 71 meters and source depth of 24 meters).

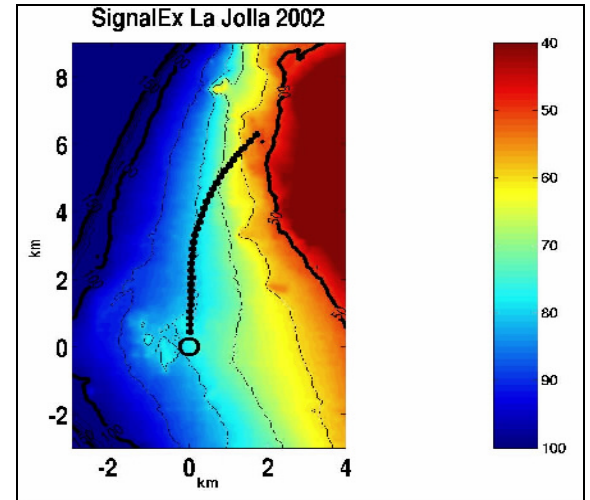


Figure 6. SignalEx La Jolla 2002 experiment configuration.

III. MODELING

Figure 6 shows the bathymetry off the coast of La Jolla where the experiment was performed. The bathymetry between the receiver (indicated by the circle) and the drifting source (whose track is marked by dots) is reasonably flat, at least for the first 3-4 kilometers, before the source veers to the right. A single radial from the fixed receiver was used to set the bathymetry that was used in the model. Figure 7 shows the measured sound speed profile and the depths of the source (24 meters) and receiver (71 meters).

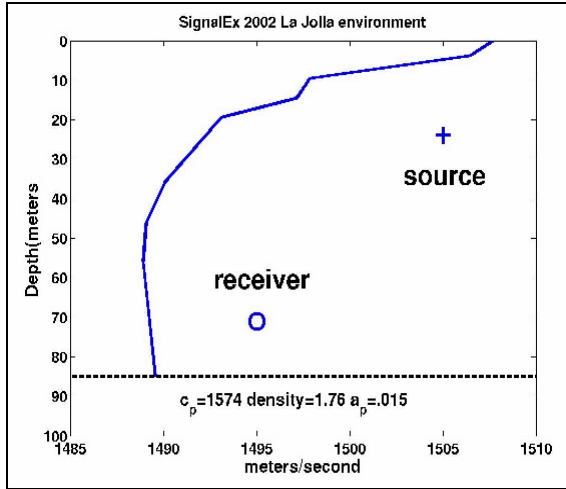


Figure 7. SignaleX La Jolla 2002 environment.

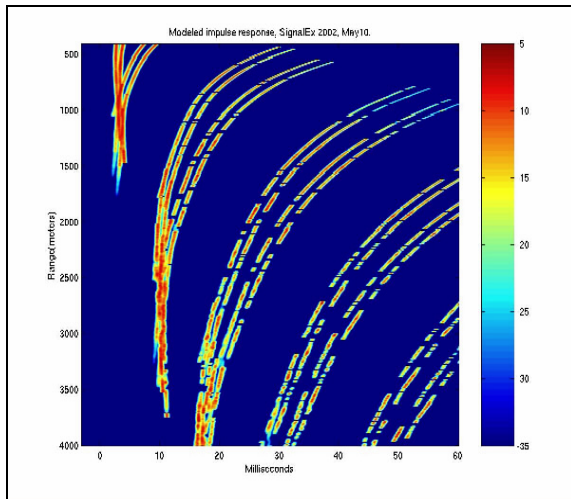


Figure 8. Modeled channel impulse response as a function of range (receiver depth of 71 meters and source depth of 24 meters).

To reproduce the range-dependent impulse response function shown in Figure 5, the broadband channel impulse response function was modeled using the Bellhop ray/beam tracing program (see [18], [19], and [20]). This model calculates magnitudes, phases (although only envelopes are shown in the plots of modeling calculations below), and times of travel of all multipath components for a particular source and receiver geometry (source depth, source-to-receiver range, and receiver depth), given a sound speed profile, properties of the surface and bottom, and a potentially range-dependent bathymetry. A band-limited impulse response function is synthesized from these multipath arrival parameters.

Figure 8 shows the multipath structure calculated by Bellhop for the experiment configuration during the La Jolla SignalEx test (relative time of arrival is shown along the horizontal axis, and range along the vertical axis, range being calculated from GPS measurements). The agreement between the coarse features of Figure 5 and Figure 8 is excellent, which bodes well for our model-based source localization.

However, the later arrivals in the measured data, whose relative time of arrival exhibits the fluctuations seen in Figure 3 and Figure 4, have been smeared out by the averaging process, resulting in the amplitudes of the later arrivals in Figure 5 being underestimated, compared to the modeled amplitudes of the later arrivals in Figure 8.

Figure 9 and Figure 10 show blowups of the measured and modeled data (seen in Figures Figure 5 and Figure 8), showing what happens to the impulse response over ranges from 400 to 1600 meters. Note that from 1000 to 1400 meters there is a pair of earliest arrivals that is not predicted by the ray model. Note too that from 600 to 1200 meters, the later set of arrivals (at 10 and 20 milliseconds in Figure 9) show significant fading that is not predicted by the ray model. These differences between the measured and modeled data can be expected to cause problems for any source localization based on matching this measured and modeled data.

The dropouts seen along some of the later arrivals in the modeled data are due to the range-dependent bathymetry. These were duplicated by a broadband parabolic equation calculation, run as a check on the ray tracing results. Because the measured data is the result of averaging over 25 seconds of drift, these dropouts are not observed in the measured data.

Comparing the measured and modeled impulse response functions, and given the fluctuations in the times of arrival and amplitudes and how they vary among the different multipath arrivals, it is not obvious what form the optimal source location estimate should take.

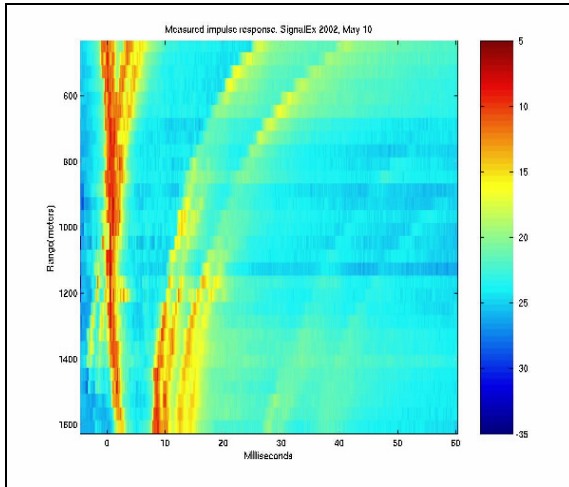


Figure 9. Measured impulse response to 1600 meters range.

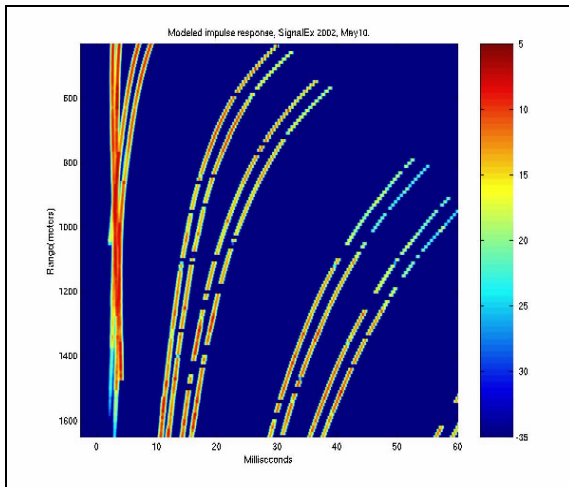


Figure 10. Modeled impulse responses to 1600 meters range.

IV. LOCALIZATION

The source localization metric or statistic (also called an ambiguity surface) is calculated for every candidate source location (i.e. we search in range and depth) by cross-correlating the measured and modeled impulse response functions and selecting the maximum cross-correlation peak. A cross-correlation is necessary, because we do not have a time reference for the measured data, and as a result must examine every possible lag or offset between the measured and modeled impulse response functions. This calculation produces a value for every candidate source range and depth, at every time epoch for which we have measured the impulse response (as the source drifts in range). Thus a 2D ambiguity surface is produced for each time epoch, and the overall output for the entire source drift is a 3D ambiguity volume, indexed on source range, source depth, and time epoch. Figure 11 shows the 2D slice versus range and time for the known source depth of 24 meters. The circles indicate the known source range, calculated from GPS measurements at each time epoch. The range track is consistent with the GPS measurements. Figure 12 shows the slices

versus depth that follow the source track in range. A very strong track is apparent at the known source depth of 24 meters. A persistent track is apparent in both range and depth.

Our previous experience working with broadband signatures at lower frequencies showed that it was significantly more difficult to model the phases of the multipath components than the envelopes and times of arrival. We had mixed results matching on both magnitude and phase, even on low frequency data. Given reasonably accurate information about the bottom (enough to predict the critical angle) and about the sound speed profile in the water column, it was possible to consistently reproduce the envelope of the multipath pattern. However, in the high frequency band being addressed here, simply matching the modeled and measured impulse response envelopes only produced a plausible source track for a few short ranges (starting at 400 meters). There were several reasons for this. Looking at the measured and modeled data, the mismatch in the higher amplitude earlier arrivals was dominating the information provided by the later arrivals. This was further compounded by the later arrivals being smeared out by our averaging process, due to the fluctuations in their time of travel.

Reference [16] used the log envelope of the measured and modeled waveforms being matched to emphasize the contribution of the later arrivals. With a similar motivation, the measured and modeled impulse response waveforms were similarly remapped prior to matching. The measured waveform was whitened using a three-pass, split-window moving average process to estimate both the mean and the standard deviation at each sample. The modeled waveform was raised to a fractional power (.1) in order to reduce the disparity between the early and late arrival amplitudes. These somewhat ad hoc transforms resulted in the much improved results shown in Figure 11 and Figure 12.

Note that although we have taken great pains in the previous sections to align the measured impulse response functions so that their structure versus range is very apparent, the source localization algorithm discussed in this section is not sensitive to this alignment, because it operates on each matched filter output independently of all others, and seeks the maximum amplitude in the cross-correlation of the measured and modeled envelopes (so it checks all possible lags between the measured and modeled impulse response functions). The modeled results are displayed using a reduced time (range/sound speed) to set the left edge of each image row. The measured response functions are displayed using a detected early arrival to set the left edge of the first image row, and the peak cross-correlation (row to row) to set subsequent rows (as discussed above).

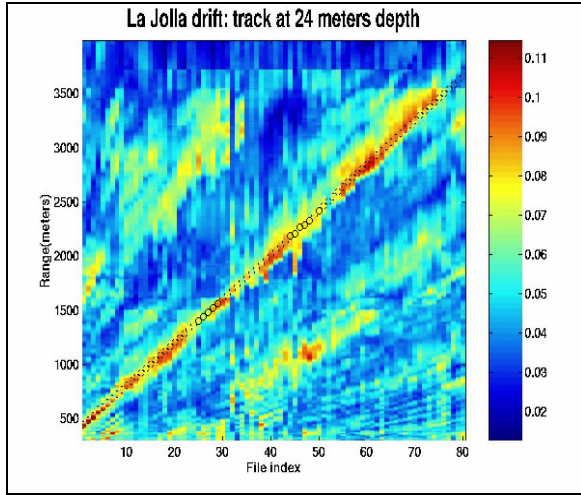


Figure 11. Range track at source depth of 24 meters (and receiver depth of 71 meters).

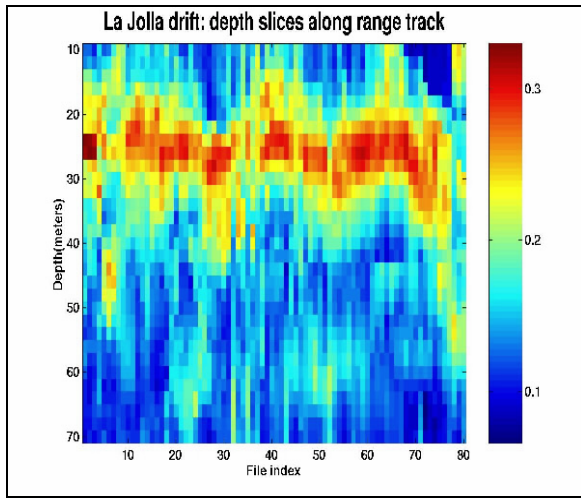


Figure 12. Depth track for source range track shown in Figure 11.

V. DISCUSSION AND CONCLUSIONS

The most striking finding is that there seems to be a stable, exploitable impulse response of distinct and predictable multipath arrivals at these high frequencies. Although we only show results for a single site, we have seen qualitatively similar results at a number of sites where SignalEx experiments were performed.

The measured impulse response can be reproduced by standard acoustic propagation models well enough to support source localization using a single point receiver, although this was much more difficult than we have found at low frequencies (see [17]).

Admittedly, using a known source waveform to measure the impulse response would not be possible with an uncooperative source. However, we have had no trouble extending similar time-domain based source localization to a source waveform unknown scenario (at low frequencies, see [17]) by matching measured and modeled correlation waveforms. This requires a reasonably wideband source signature and pre-whitening if the signature is

not smooth in the frequency domain. Figure 13 shows the cross correlation of two Telesonar Testbed receive elements, from the SignalEx La Jolla experiment (the same data we used to demonstrate source localization in the previous sections), showing a rich multipath structure. The same model used for the impulse response above can reproduce this structure. Note that a correlation waveform has an implicit time reference, so the matching consists of an inner product as opposed to a cross-correlation, as was needed to match impulse response waveforms.

Note that working in the time-domain enabled us to deal directly with the fluctuations in the impulse response caused by surface motion and bottom bathymetry.

Acknowledgment

The SignalEx experiments were funded by ONR.

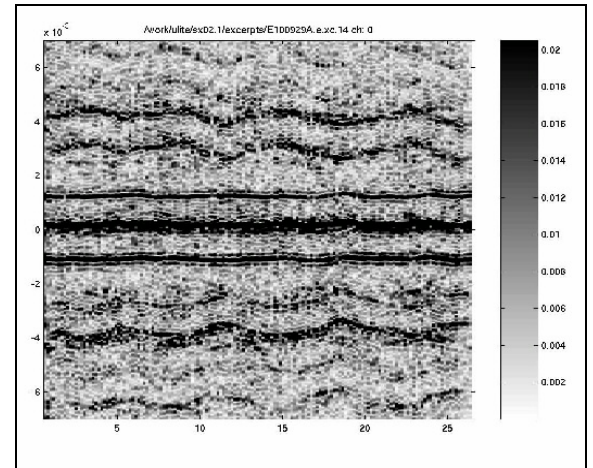


Figure 13. Cross-correlation measured from 2 of 4 testbed receive elements, spaced for diversity.

REFERENCES

- [1] H. P. Buckner, "Use of calculated sound fields and matched-field detection to locate sound sources in shallow water", *J. Acoust. Soc. Am.*, vol. 59, pp. 368-373, 1976.
- [2] A. B. Baggeroer, W. A. Kuperman, P. N. Mikhalevsky, "An overview of matched-field methods in ocean acoustics", *IEEE J. Oceanic Eng.* **OE-18**(4):401-424 (1993).
- [3] N. O. Booth, P. A. Baxley, J. A. Rice, P. W. Schey, W. S. Hodgkiss, G. L. D'Spain, and J. J. Murray, "Source localization with broad-band matched-field processing in shallow water", *IEEE J. Oceanic Eng.*, **21**(4), 402-412 (1996).
- [4] A. Parvulescu, "Signal detection in a multipath medium by M.E.S.S. processing," *J. Acoust. Soc. Am.*, **33**, 1674- (1961).
- [5] A. Parvulescu and C. S. Clay, "Reproducibility of signal transmissions in the ocean," *Radio Electron. Eng.*, vol. 29, pp. 223-228, 1965.
- [6] L. Nghiem-Phu, F. D. Tappert, and S. C. Daubin, "Source localization by CW acoustic retrogration," *Proceedings of a Workshop on Acoustic Source Localization*, internal NRL report, ed: R. Fizell, (1985).
- [7] D. R. Jackson and D. R. Dowling, "Phase conjugation in underwater acoustics," *J. Acoust. Soc. Am.*, vol 89, pp. 171-181, 1991.
- [8] Zoi-Heleni Michalopoulou and M. B. Porter, "Matched-field processing for broad-band source localization", *IEEE Journal of Oceanic Engineering*, vol. 21, no. 4, pp. 384-392, October, 1996.
- [9] Z. H. Michalopoulou, M. B. Porter, and J. Ianniello, "Broadband source localization in the Gulf of Mexico", *Journal of Computational Acoustics*, **2**(3),361-370 (1996).
- [10] J. P. Ianniello, "Recent developments in SONAR signal processing", *IEEE Signal Processing Magazine*, **15**(4):27-40 (1998).
- [11] R. K. Brienzo and W. S. Hodgkiss, "Broadband matched-field processing", *J. Acoust. Soc. Amer.*, **94**(5), 2821-2831 (1993).
- [12] E. K. Westwood, "Broadband matched-field source localization", *J. Acoust. Soc. Amer.*, **91**(5):2777-2789 (1992).
- [13] S. M. Jesus, "Broadband matched-field processing of transient signals in shallow water", *J. Acoust. Soc. Amer.*, **93**(4):1841-1850 (1993).
- [14] E. K. Westwood and D. P. Knobles, "Source track localization via multipath correlation matching", *J. Acoust. Soc. Amer.*, **102**(5), 2645-54 (1997).
- [15] W. S. Hodgkiss, W. A. Kuperman, J. J. Murray, G. L. D'Spain and L. P. Berger, "High Frequency Matched Field Processing", from "High Frequency Acoustics in Shallow Water", ed. N. G. Pace, E. Pouliquen, O. Bergem and A. P. Lyons, NATO SCALANT Undersea Research Centre, pp. 229-234, 1997.
- [16] M. B. Porter, S. Jesus, Y. Stéphan and X. Démoulin, E. Coelho, "Exploiting reliable features of the ocean channel response", *Shallow Water Acoustics*, R. Zhang and J. Zhou, Eds., China Ocean Press, p. 77-82, Beijing, China (1998).
- [17] M. B. Porter, Paul Hursky, Christopher O. Tiemann, Mark Stevenson, "Model-based tracking for autonomous arrays", *MTS/IEEE Oceans 2001 – An Ocean Odyssey, Conference Proceedings*, pp. 786-792, Honolulu, Hawaii, November 5-8, 2001.
- [18] M. B. Porter, Acoustics Toolbox, at <http://oalib.saic.com/Modes/AcousticsToolbox>.
- [19] M. B. Porter, "Acoustic Models and Sonar Systems," *IEEE J. of Oceanic Engineering*, Vol. OE-18(4):425-437 (1994).
- [20] F. Jensen, W. A. Kuperman, M. B. Porter and H. Schmidt, *Computational Ocean Acoustics*, Springer-Verlag, (2000).